Electronic Supplementary Material (ESI) for Materials Horizons.

This journal is © The Royal Society of Chemistry 2018

Supporting Information

A Self-Healing Hydrogel with Pressure Sensitive Photoluminescence for Remote Force Measurement and Healing Assessment

Ming Li,‡[a] Weijun Li,‡[a] Wei Cai,[a] Xiaojie Zhang,[a] Zhihang Wang,[a] Jason Street,[b] Wee-Jun Ong,*[c,d] Zhenhai Xia,[e] Quan Xu*[a]

[a]*State Key Laboratory of Heavy Oil Processing, China University of Petroleum-Beijing, 102249, China. E-mail: xuquan@cup.edu.cn*

[b]*Department of Sustainable Bioproducts, Mississippi State University, Mississippi, 39762, USA*

[c]*School of Energy and Chemical Engineering, Xiamen University Malaysia, Selangor Darul Ehsan 43900, Malaysia. Email: weejun.ong@xmu.edu.my; ongweejun@gmail.com Web: sites.google.com/site/wjongresearch/*

[d]*College of Chemistry and Chemical Engineering, Xiamen University, Xiamen 361005, China*

[e]*Department of Materials Science and Engineering and Department of Chemistry, University of North Texas, Denton, Texas 76203, United States*

† Electronic supplementary information (ESI) available: the description of various testing methodologies, characterizations, experimental mechanisms, and explanations of this material can be seen in Table S1-S3, Fig. S1-S32 and Video S1-S5.

‡ The two authors contribute equally to this work.

Table S1. Cytotoxicity reaction grading table.

Reaction grading	Relative proliferation rate (%)
Level 0	≥100
Level 1	80~99
Level 2	50~79
Level 3	30~49
Level 4	0~29

Table S2. Cytotoxicity test results of Prostate Cancer Cells (PC3) extraction in each group.

Group	Values of absorption at 570 nm	Values of absorption at 630 nm	Difference of absorption between 570 nm and 630 nm	Relative growth rate (%)	Cytotoxicity grade
Blank control	0.914±0.026	0.216±0.022	0.698±0.024	100	0
Negative control	0.876±0.037	0.227±0.014	0.649±0.026	93	1
Positive control	0.141±0.003	0.043±0.005	0.098±0.004	14	4
Original extraction	0.738±0.024	0.166±0.012	0.572±0.018	81.9	1
50% dilution	0.854±0.041	0.216±0.013	0.638±0.027	91.4	1

Supplementary explanation

Cytotoxicity test:

Sample: Prostate cancer cells (PC3)

Preparation of different extracts. Leaching solution group: Under aseptic conditions, a sample surface area of 15 cm^2 was used, cell culture medium was added and 5 mL of prostate cancer cells (PC3) 15% by volume were added and the sample was incubated for 24 h at 37 °C.

50% extracting solution group: The sample extract was diluted 1 time.

Negative control group: High-density polyethylene with a surface area of 30 cm^2 was used, 5.0 mL of cell culture solution was added and the sample was incubated at 37 °C for 24 h.

Positive control group: 5.0 mL of cell culture medium containing 5 g/L phenol was used and incubated at 37 °C for 24 h.

Blank control group: 5.0 mL of cell culture medium was used and incubated at 37 °C for 24 h.

Preparation of cell suspension: The normal subcultured PC3 cells were digested with digestive juice to prepare a cell suspension with a concentration of 1×10^7 L^{-1}, and seeded on a 96-well plate, with 100 μL/well and 6 wells per group. The suspension was cultured in a CO_2 incubator (37 ° C, volume fraction of 5% CO_2).

Extraction of the extract: After the cells were cultured for 24 h, the original cell culture solution was discarded, and the test sample group was exchanged with the extract solution and the 50% extract solution respectively; the blank control group, the negative control group and the positive control group were used for the corresponding control. The liquid was exchanged and exchanged in a CO_2 incubator.

Determination of absorbance and cytotoxicity: 20 μL of 5 g/L tetramethylazozolium salt solution was added to each well to continue the culture after 72 h of culture time. After 4 h, the liquid in the well was discarded and 150 μL of dimethyl was added, then sulfone was shaken on a shaker for 10 min, and the absorbance at 570 nm and 630 nm was measured with a microplate reader. The relative growth rate (RGR) of the cells was calculated by the following formula: $RGR = (A/A_0) \times 100\%$. A is the difference between the absorbance at 570 nm and 630 nm in the sample group (leaching solution group, 50% extract solution group, negative control group, positive control group); A_0 is the difference between the absorbance at 570 nm and 630 nm in blank control group. According to the magnitude of the relative proliferation rate, the corresponding toxicity level was found (Table S1).

Table S3. Comparison of the self-healing hydrogels in this study to other self-healing materials from the literature.

Self-healing material	Maximum stress	Healing time	Healing efficiency	Healing in water	Healing in other solution	Stimulating	References
PVA/Chitosan/ Agarose/glycerol	10.21 MPa	30 s	100%	60 s 90%	N-hexane; Petroleum-ether; NaCl solution	No	This study
Agarose/PVA	24.65 kPa	10 s	94.7%	60 s 70%	-	No	[1]
Eu/IDA	-	4 h	-	-	-	No	[2]
CNCs/PVA/PVP	2.1 MPa	30 min	90%	-	-	No	[3]
CEC/OSA/ADH	34 kPa	12 h	86%	-	PBS (pH = 7.0) 3 h	No	[4]
NaSS/MPTC	0.5 MPa	2 h	99%	-	-	No	[5]
Ni/DETA	0.9 MPa	5 min	99%	-	-	No	[6]
PNIPAM/PEO	-	2 min	100%	-	-	No	[7]
SDS/ UPyHCBA	8.3 kPa	30 s	99%	-	-	No	[8]
G·K^+/PDMAAm	19.2 MPa	1 min	58%	-	-	No	[9]
PS-DN	0.213 MPa	< 1min	100%	-	-	No	[10]
C8NG/PAAm	0.16 MPa	-	-	-	-	No	[11]
NapFFK/PEGMA	70 kPa	-	-	-	-	No	[12]
DN ionogel	0.95 MPa	-	-	-	-	No	[13]
Fmoc-Tyr-OH/ PDMAAm	35 kPa	-	-	-	-	No	[14]
PDGI/PAAm	-	1 min	40%	-	-	No	[15]
GG/PAAm	0.216 MPa	2 min	30%	-	-	No	[16]
Ca^{2+}-Alg/PAAm	-	24 h	74%	-	-	Heating 80 ^oC	[17]
Agar/PAAm	36 MPa	5 min	40%	-	-	Heating 100 ^oC	[18]

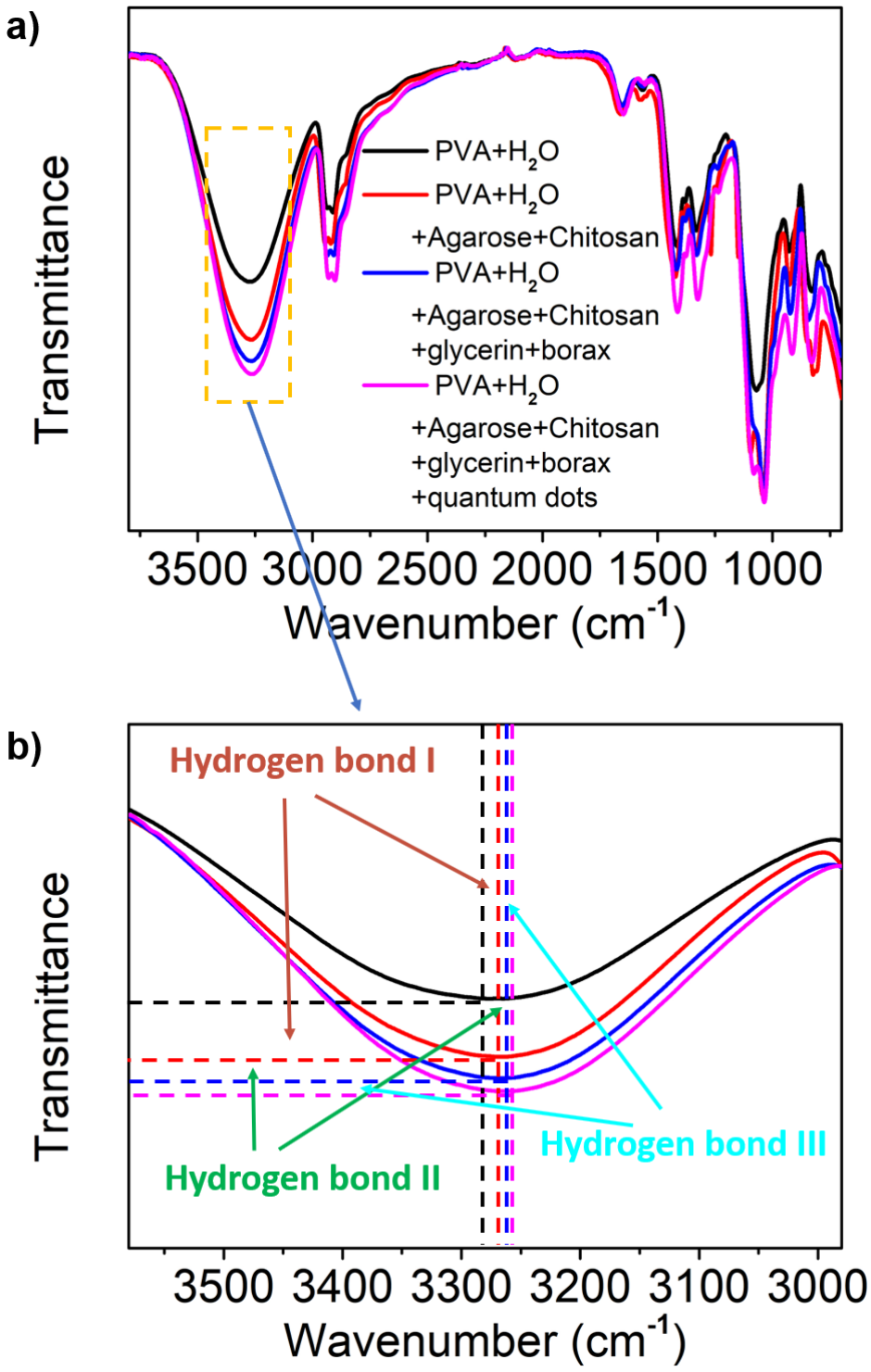

Figure S1. a) FTIR spectra of hydrogel with different components. b) Partial enlargement of Figure S1a.

Supplementary explanation

Figure S1 shows the hydrogen bond I, hydrogen bond II and hydrogen bond III in hydrogel.

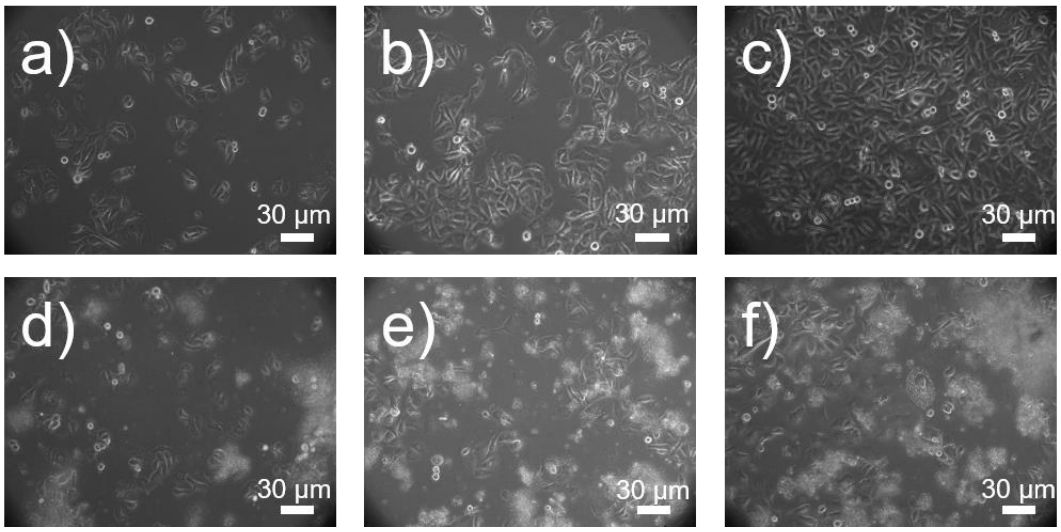

Figure S2. a) Image of prostate cancer cells after adherent growth (blank control group). b) Image of prostate cancer cells after one day of growth (blank control group). c) Image of prostate cancer cells after two days of growth (blank control group). d) Image of prostate cancer cells after adherent growth (testing group). e) Image of prostate cancer cells after one day of growth (testing group). f) Image of prostate cancer cells after two days of growth (testing group).

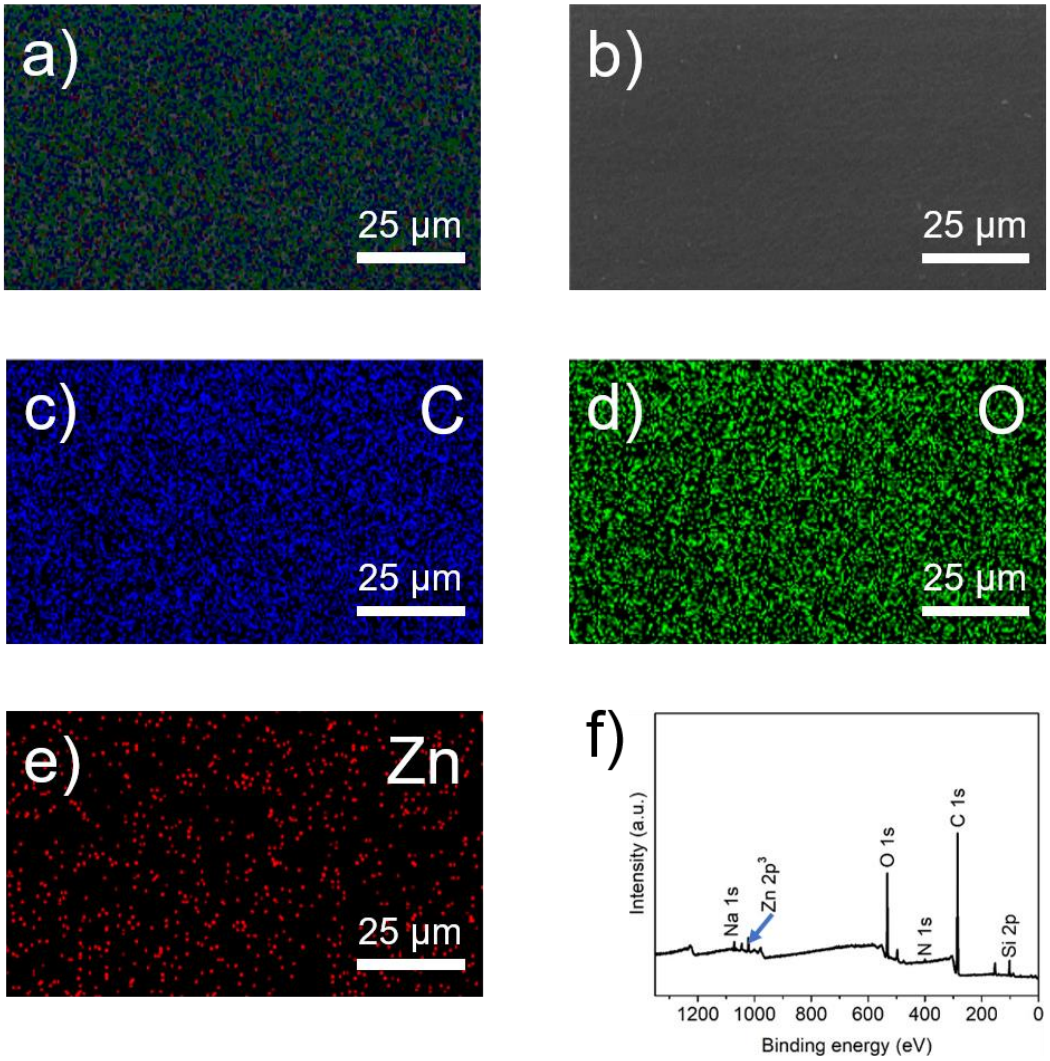

Figure S3. a) EDS layered image of hydrogel. b) SEM image of hydrogel. c) Distribution image of element C in hydrogel. d) Distribution image of element O in hydrogel. e) Distribution image of element Zn in hydrogel. f) XPS survey spectrum analysis of hydrogel.

Supplementary explanation

The raw materials (agarose, chitosan, PVA, glycerol, sodium tetraborate) used in the as-synthesized hydrogel mainly contained C, H, O, N, B and Na elements (Figure S3f). The Zn element is the feature element that we added to the blue quantum dots in order to determine the distribution of quantum dots in hydrogel. As can be seen from Figure S3e, the quantum dots were evenly distributed in the hydrogel.

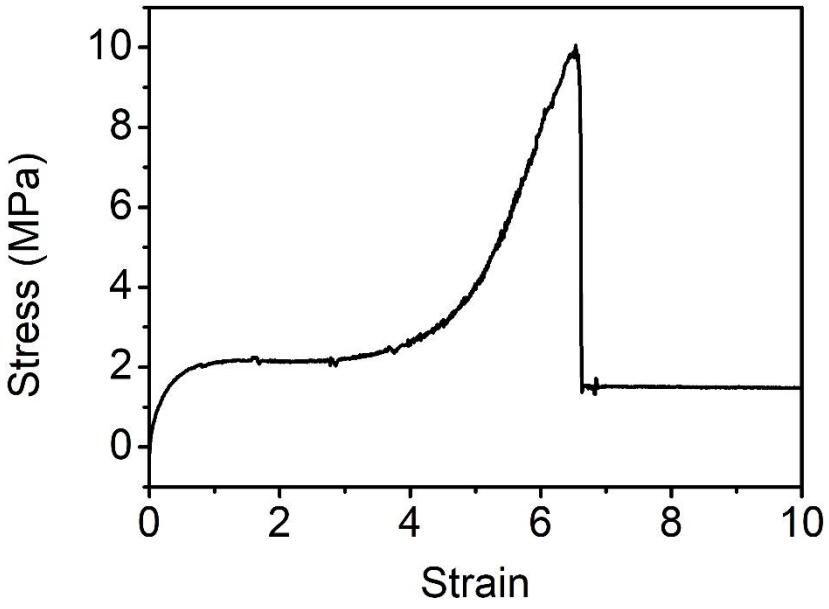

Figure S4. Tensile stress-strain curves of hydrogel with 2 mL of glycerol content.

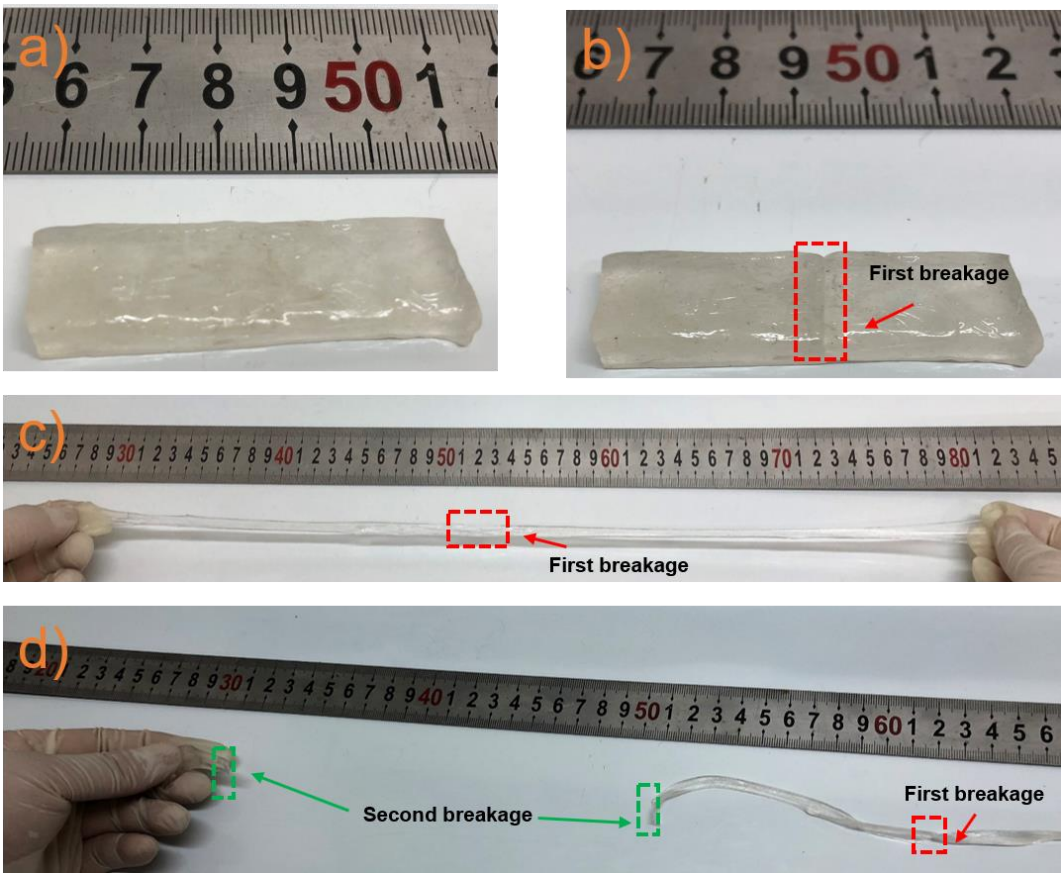

Figure S5. Self-healing photos of hydrogel in gas media. a) Photo of the initial hydrogel. b) Photo of hydrogel after being cut. c) Photograph of the stretched hydrogel after healing. d) Photograph of the hydrogel stretched to failure.

Supplementary explanation

Figure S5 shows that the location where the hydrogel underwent a secondary fracture after healing in the gaseous medium was not at the original wound location.

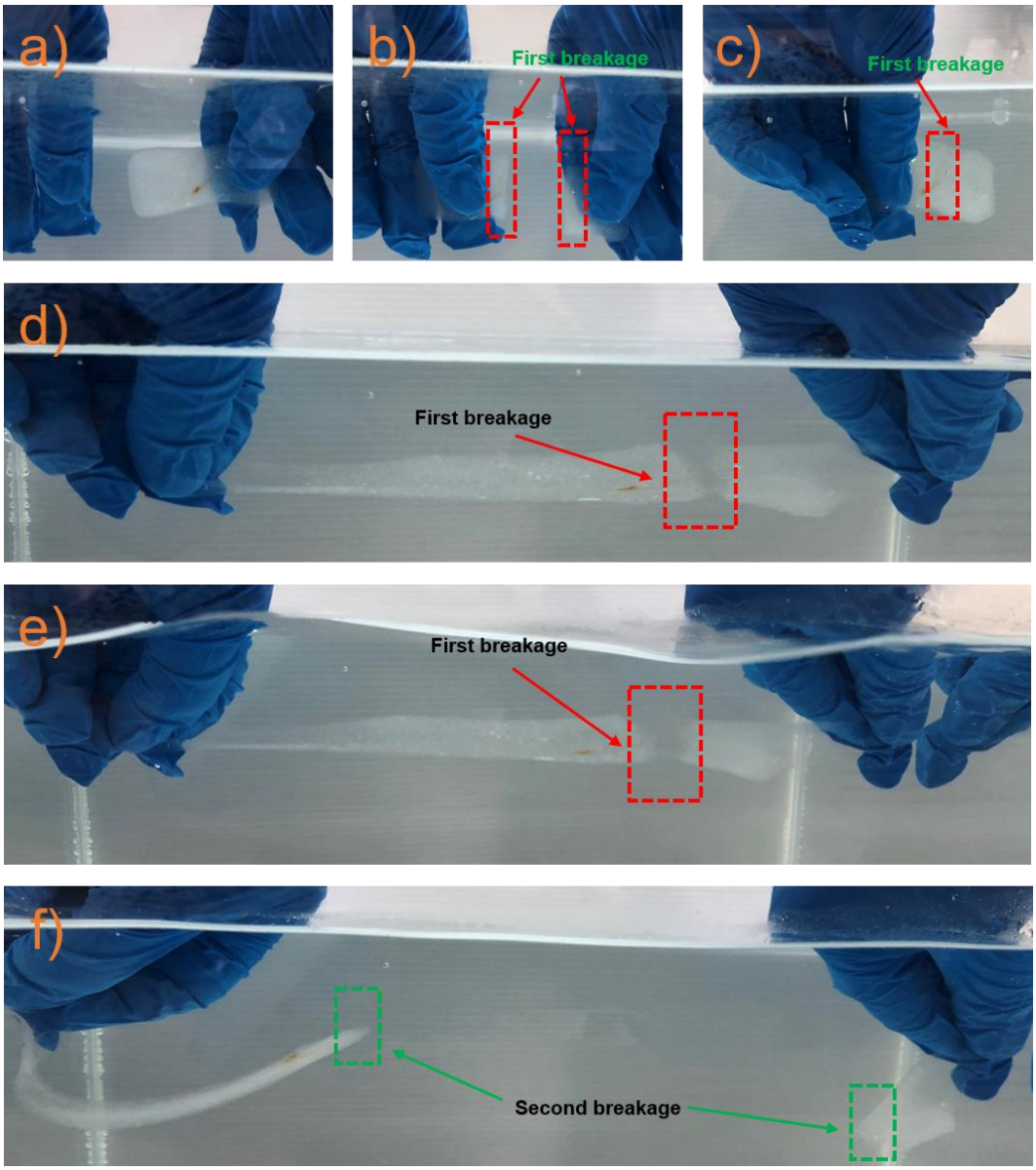

Figure S6. Self-healing photos of hydrogel in liqiud media. a) Photo of the initial hydrogel. b) Photo of hydrogel after being cut. c-e) Photograph of stretched hydrogel after healing. f) Photograph of hydrogel stretched to failure.

Supplementary explanation

Figure S6 shows the location where the hydrogel underwent secondary fracture after healing in the liquid medium was located at the original damaged position.

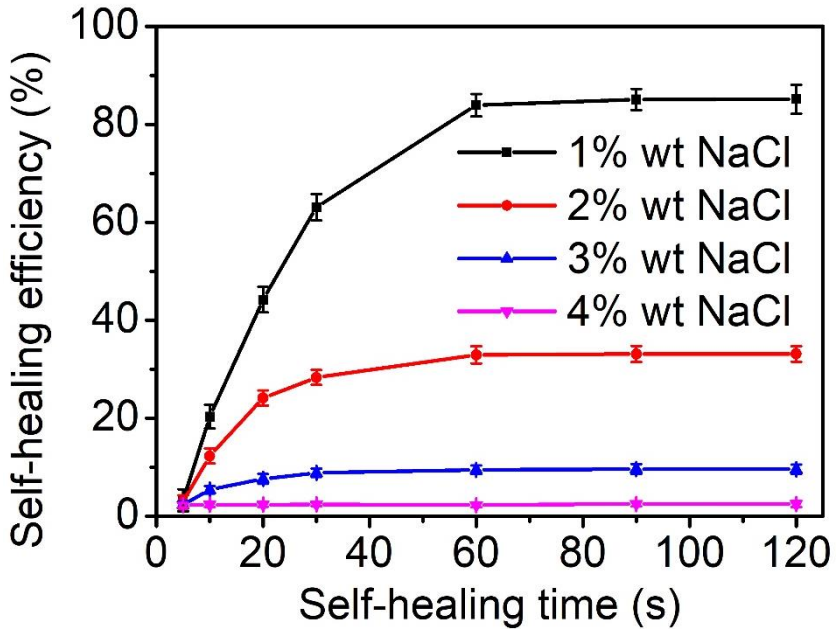

Figure S7. Relationship between self-healing efficiency and self-healing time of hydrogel with different salt concentrations.

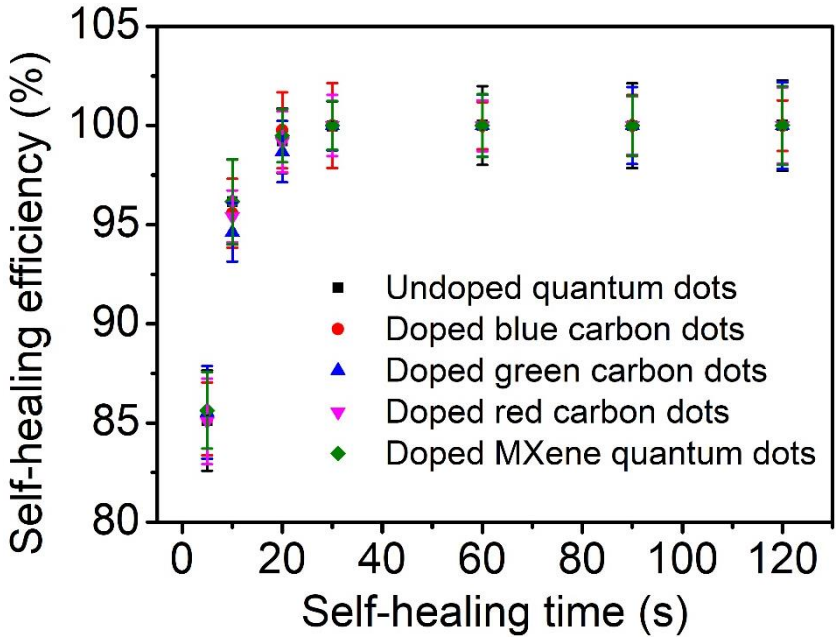

Figure S8. Relationship between self-healing efficiency and self-healing time of hydrogels which were undoped or doped with different types of quantum dots.

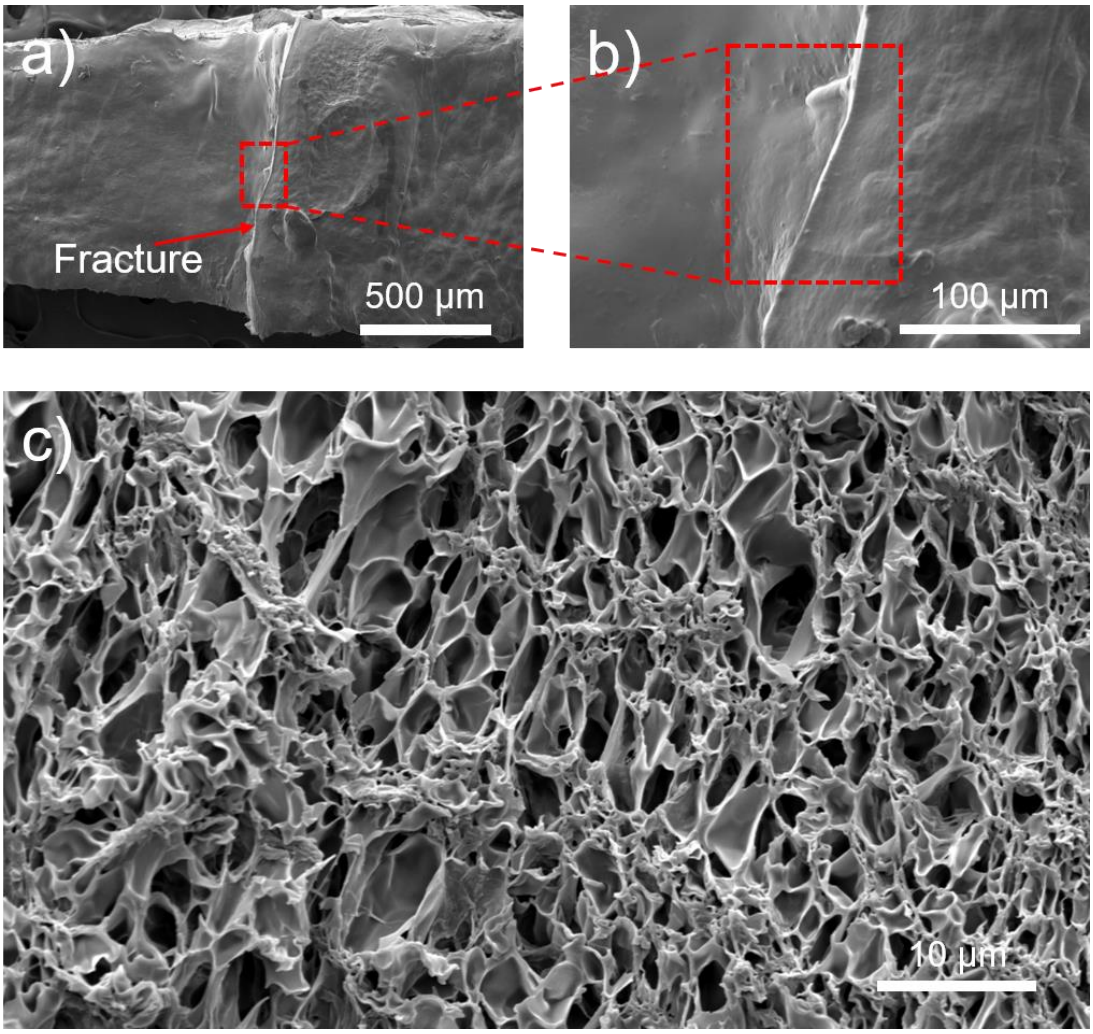

Figure S9. a, b) SEM photographs of self-repaired previously damaged location after the hydrogel underwent self-healing. c) Freeze-drying SEM image of hydrogel's structure.

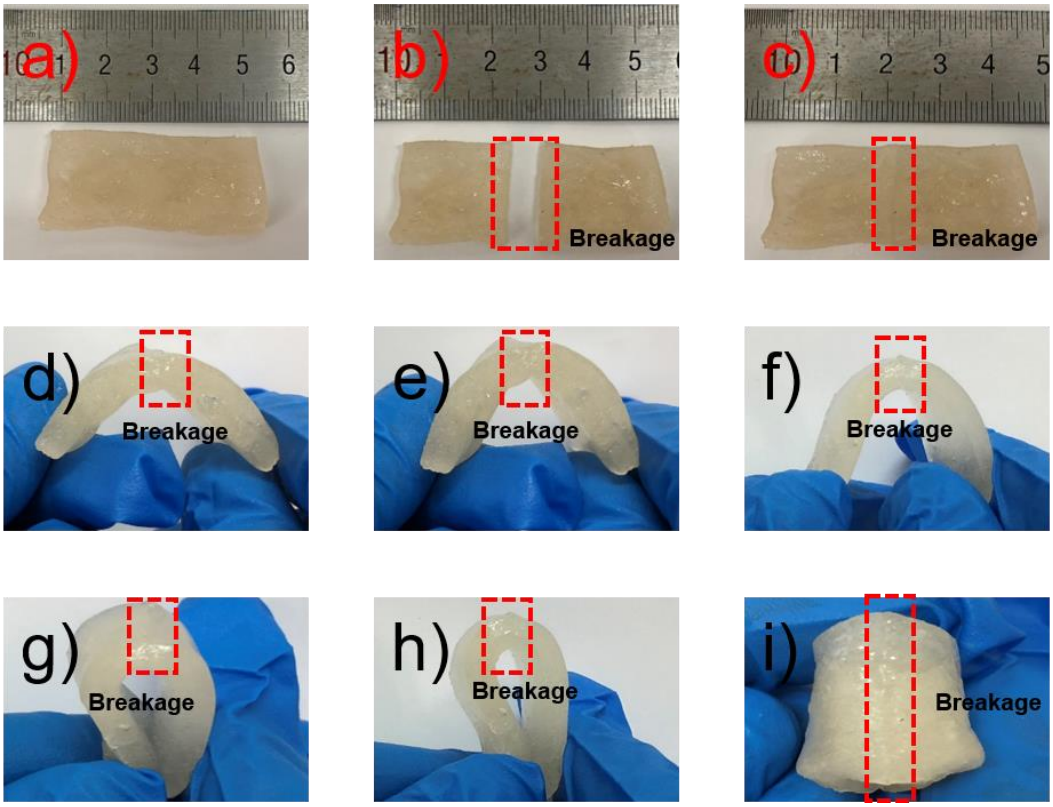

Figure S10. a) Photo of the initial hydrogel. b) Photo of hydrogel after being cut. c) Photo of hydrogel after self-healing. d-i) Different angles displaying the self-healed hydrogel.

Supplementary explanation

Figure S10 shows that the self-healing properties of the hydrogel were excellent. There was no tendency for the hydrogel to fracture after being damaged, regardless of the angle of curvature.

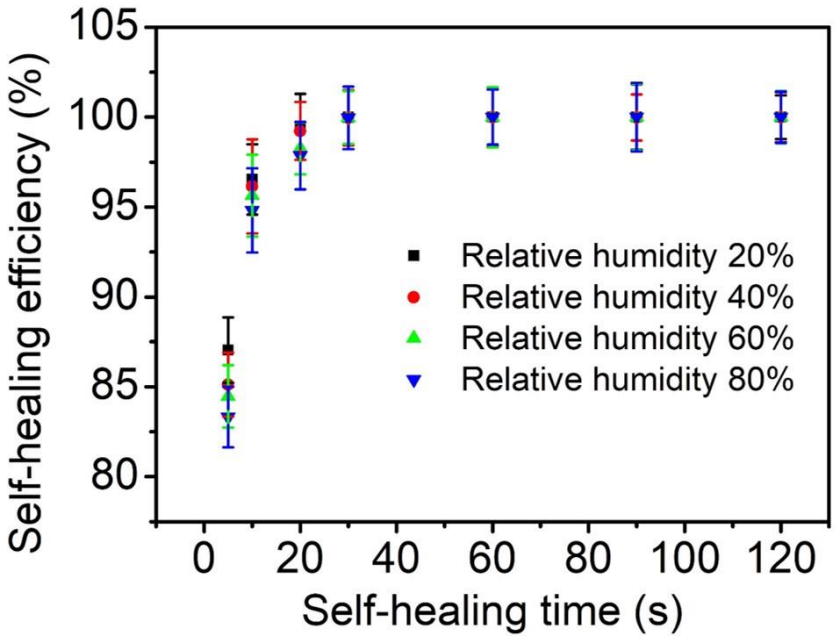

Figure S11. Relationship between self-healing efficiency and self-healing time of hydrogels with various environmental relative humidities.

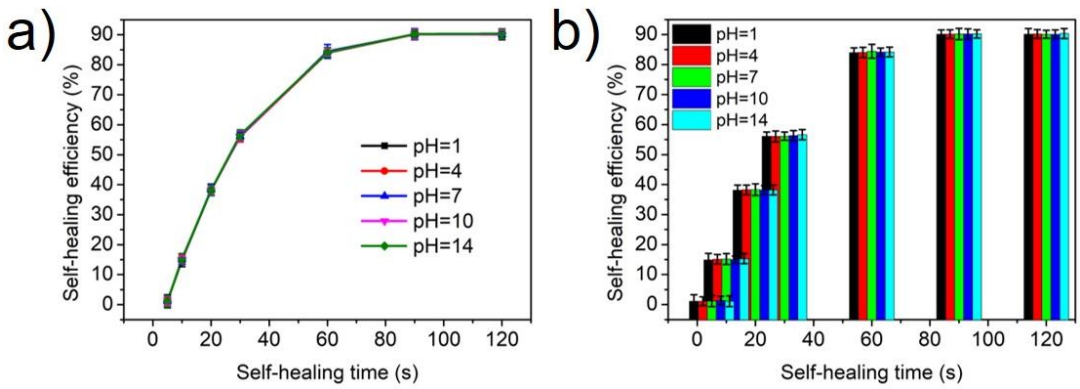

Figure S12. Relationship between self-healing efficiency and self-healing time of hydrogels in different pH solutions.

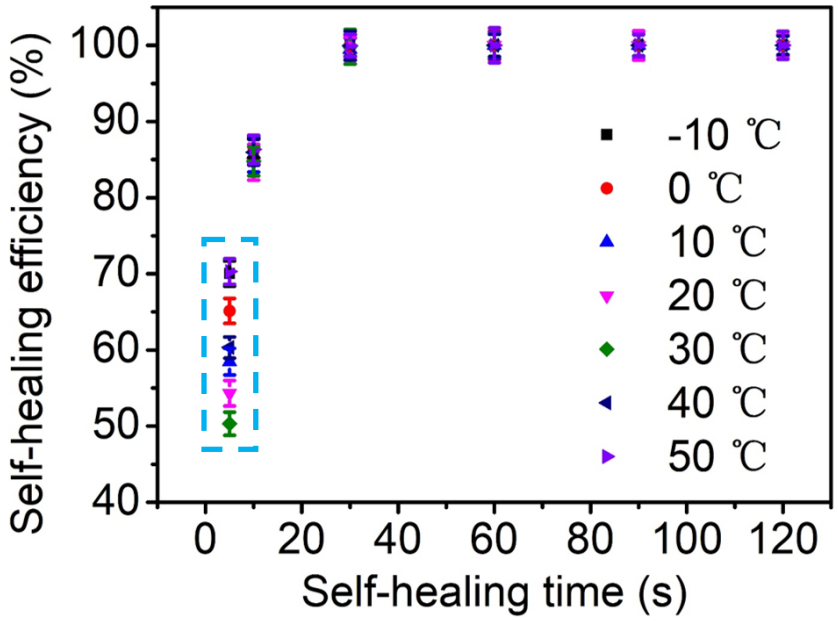

Figure S13. Relationship between self-healing efficiency and self-healing time of hydrogels with different environmental temperatures.

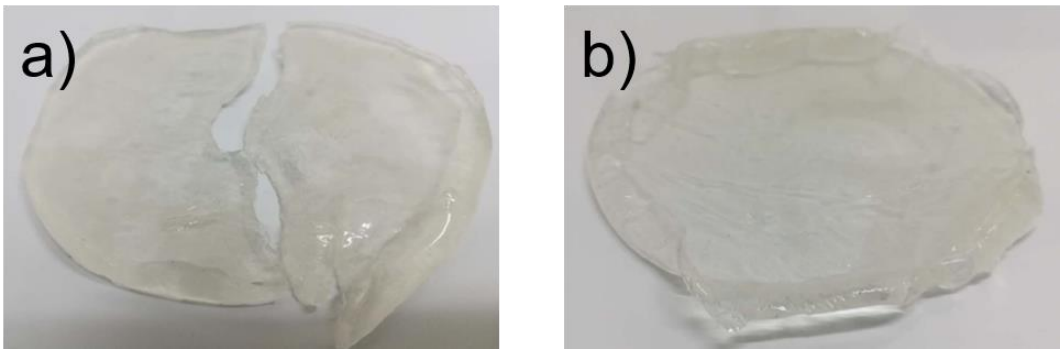

Figure S14. a) Photograph when the hydrogel was torn. b) Photograph of hydrogel after undergoing pressure remodeling.

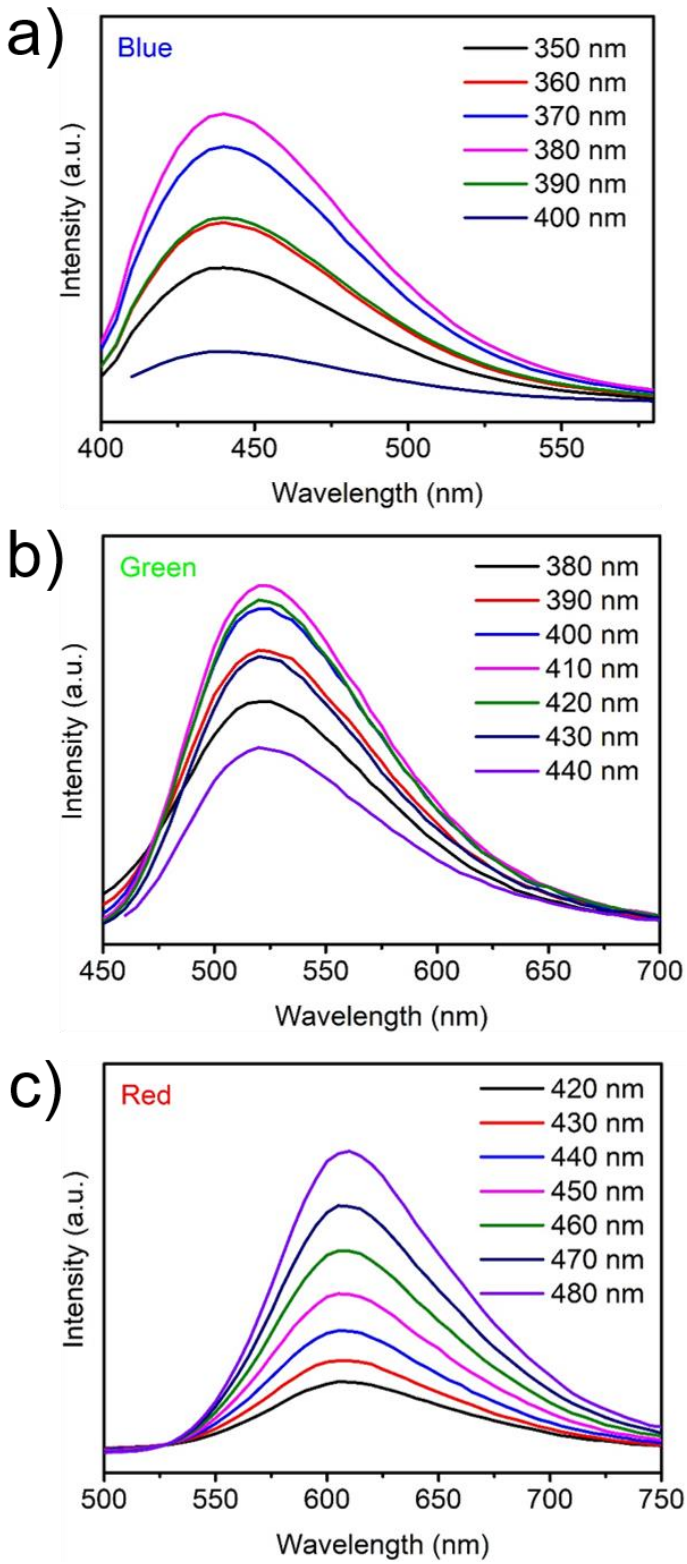

Figure S15. a) Photoluminescence spectra of blue quantum dots. b) Photoluminescence spectra of green quantum dots. c) Photoluminescence spectra of red quantum dots.

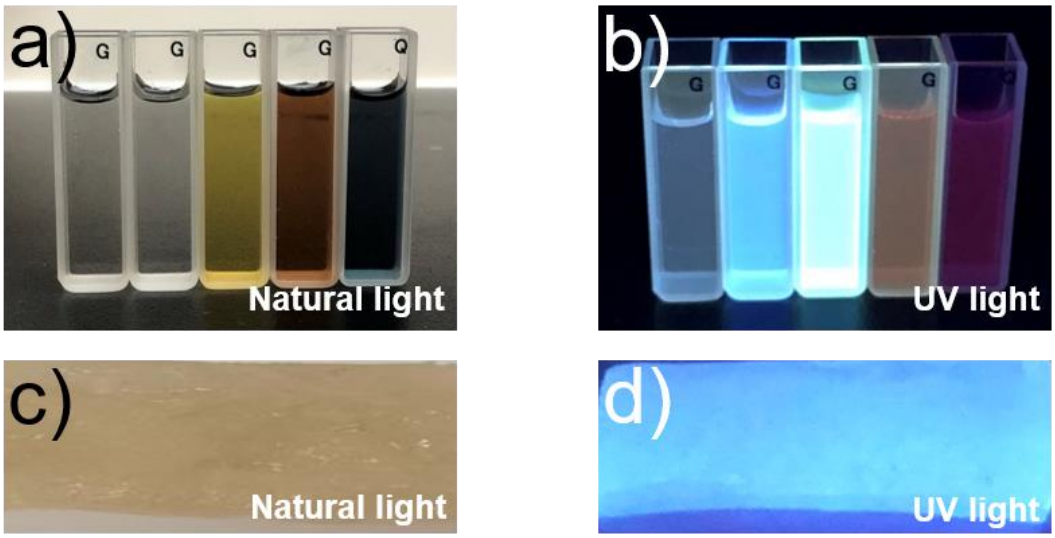

Figure S16. a) Photograph of quantum dots under natural light. b) Photograph of quantum dots under UV light. c) Photograph of a quantum dot-doped hydrogel under natural light. d) Photograph of a quantum dot-doped hydrogel under UV light.

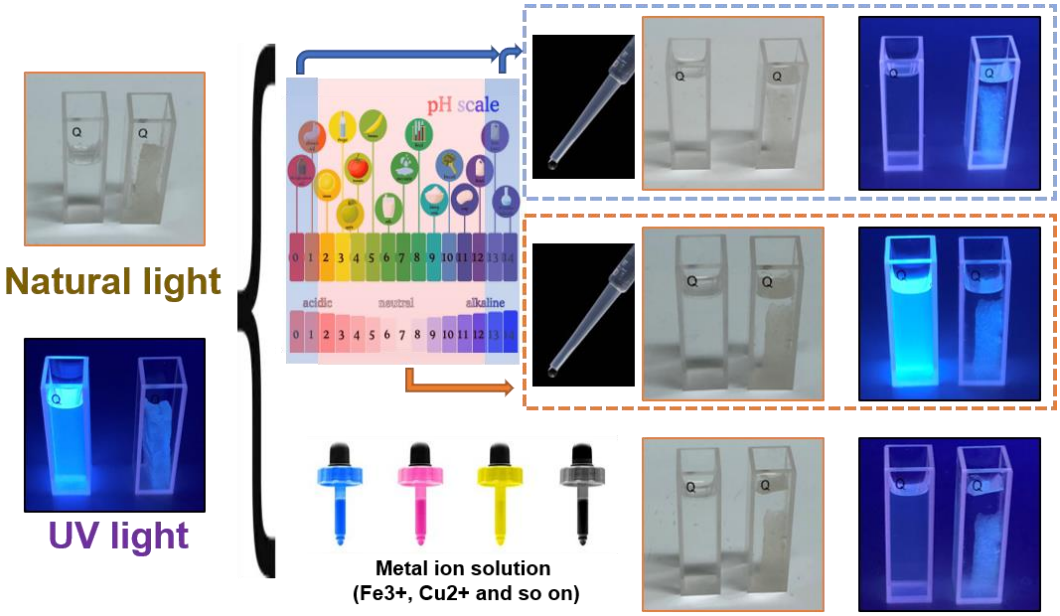

Figure S17. Luminescence status of the quantum dots solution and the quantum dots-doped hydrogel in different pH/ionic solutions.

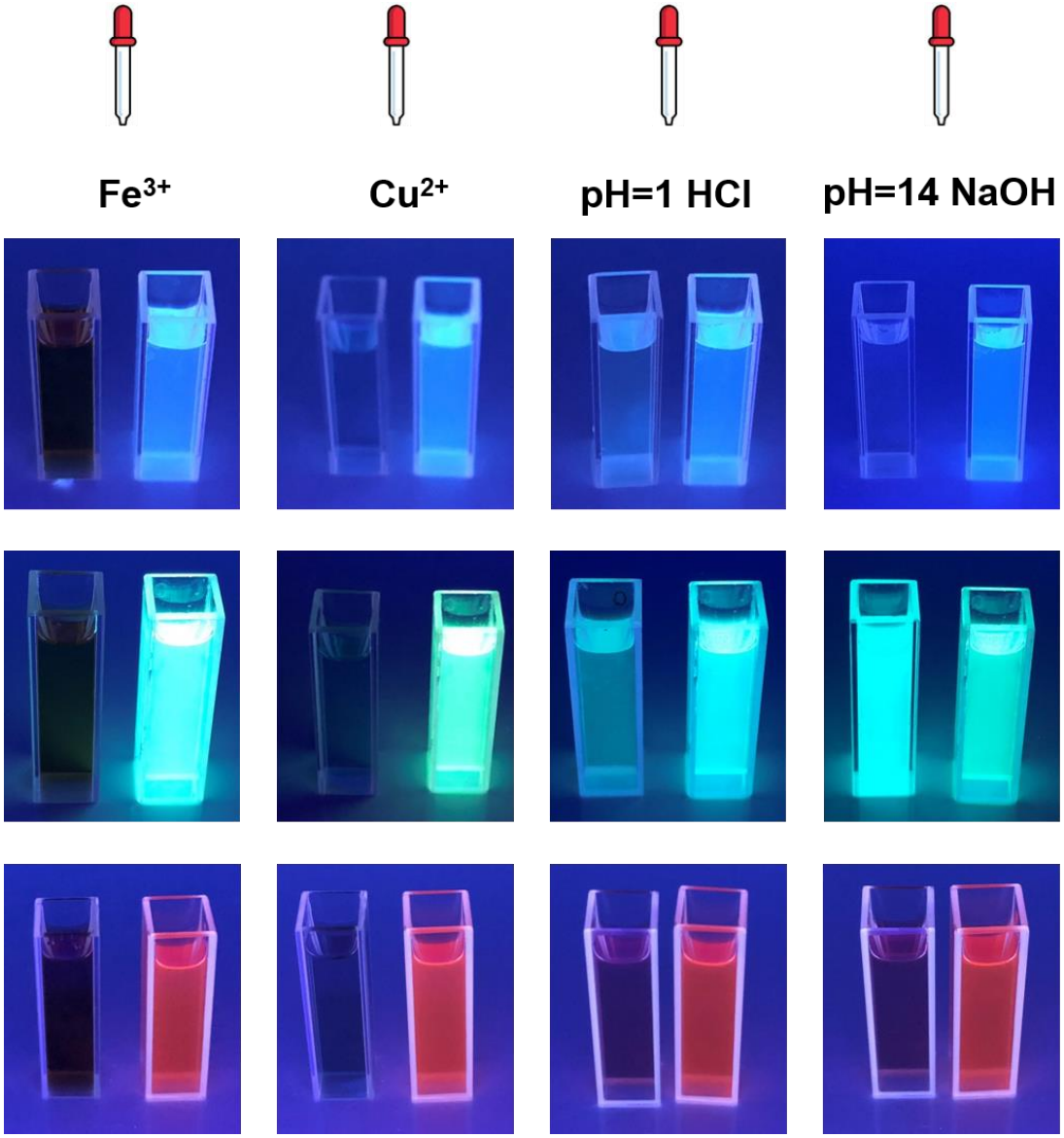

Figure S18. Deactivation status of the quantum dots solution in different pH and ionic solutions. (In each photo, the left side shows a fluorescent solution with 2 mL ions solution (0.01 mol L^{-1}) or pH solution (1 and 14) added, and the right side shows a fluorescent solution with the same amount of deionized water added.)

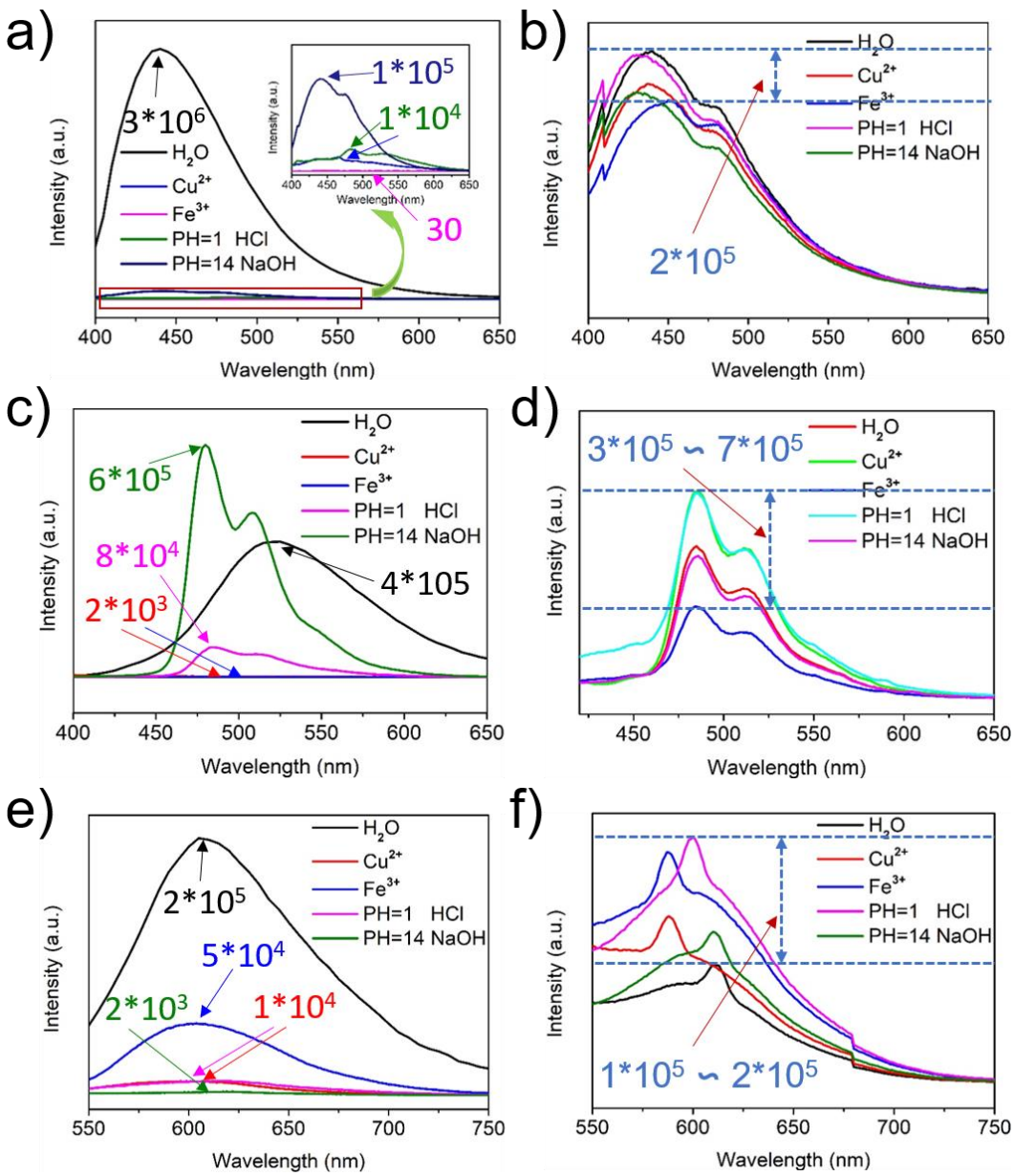

Figure S19. a) Relationship between fluorescence excitation intensity and wavelength (blue carbon quantum dots solution) in different solutions. b) Relationship between fluorescence excitation intensity and wavelength (blue quantum dots-doped hydrogel) in different solutions. c) Relationship between fluorescence excitation intensity and wavelength (green carbon quantum dots solution) in different solutions. d) Relationship between fluorescence excitation intensity and wavelength (green quantum dots-doped hydrogel) in different solutions. e) Relationship between fluorescence excitation intensity and wavelength (red carbon quantum dots solution) in different solutions. f) Relationship between fluorescence excitation intensity and wavelength (red quantum dots-doped hydrogel) in different solutions.

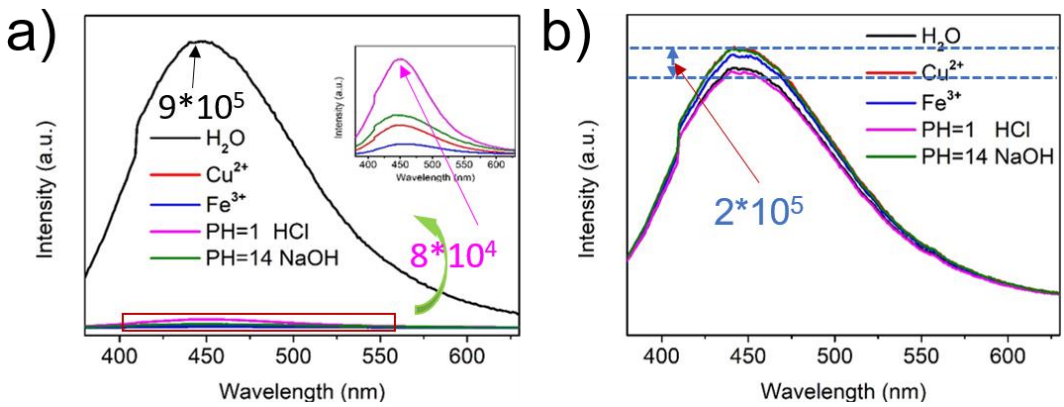

Figure S20. a) Relationship between fluorescence excitation intensity and wavelength (MXene quantum dots solution) in different solutions. b) Relationship between fluorescence excitation intensity and wavelength (MXene quantum dots-doped hydrogel) in different solutions.

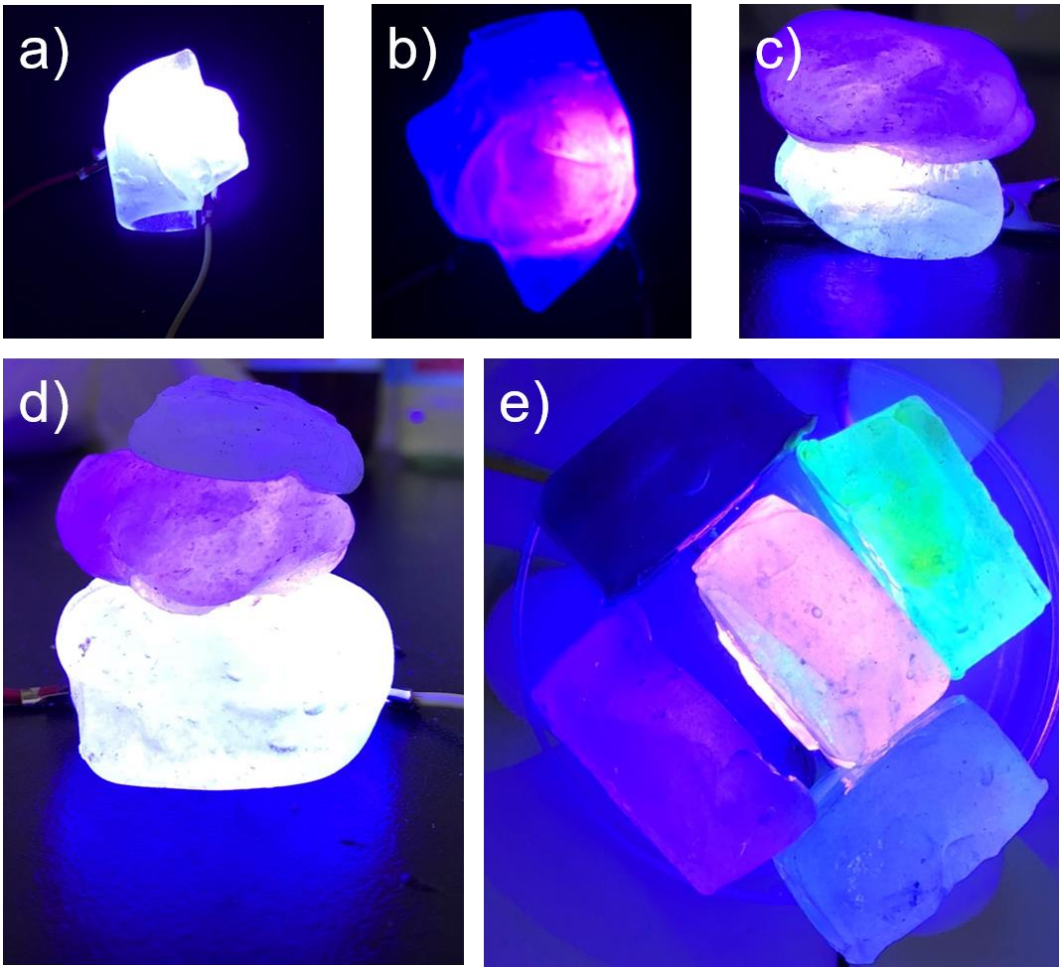

Figure S21. The color of hydrogel doped with various colors of quantum dots under the purple LED chip.

Figure S22. The color of hydrogel doped with various colors of quantum dots under natural light or the UV light/(purple LED chip).

Supplementary explanation

Figure S22 shows that by controlling the injection of quantum dots, the concentration and saturation of the quantum dot distribution in hydrogel could result in a specific pattern desired to be rendered in the hydrogel (Figure S22 ii and II).

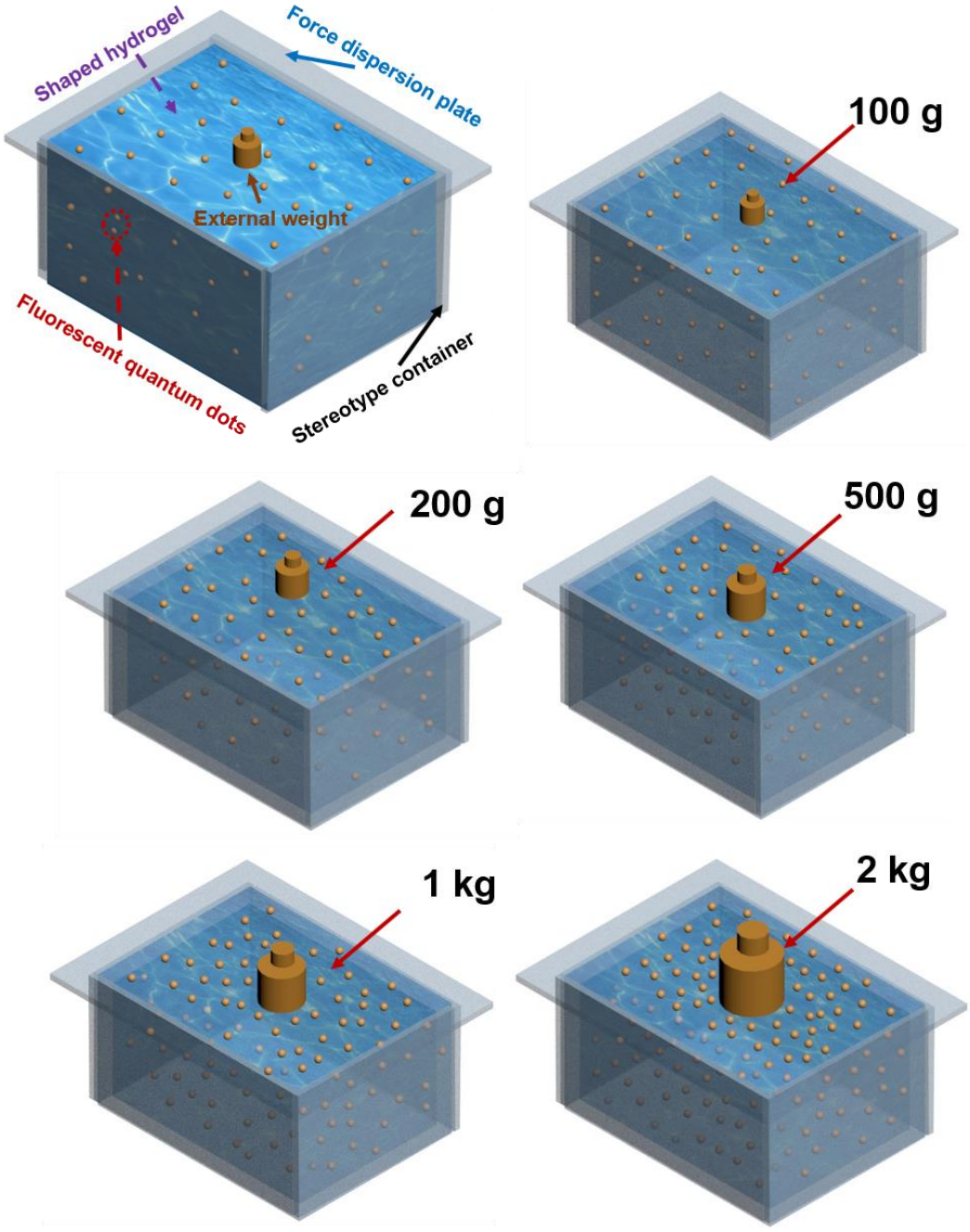

Figure S23. Schematic of subjecting the hydrogel structure under different external forces.

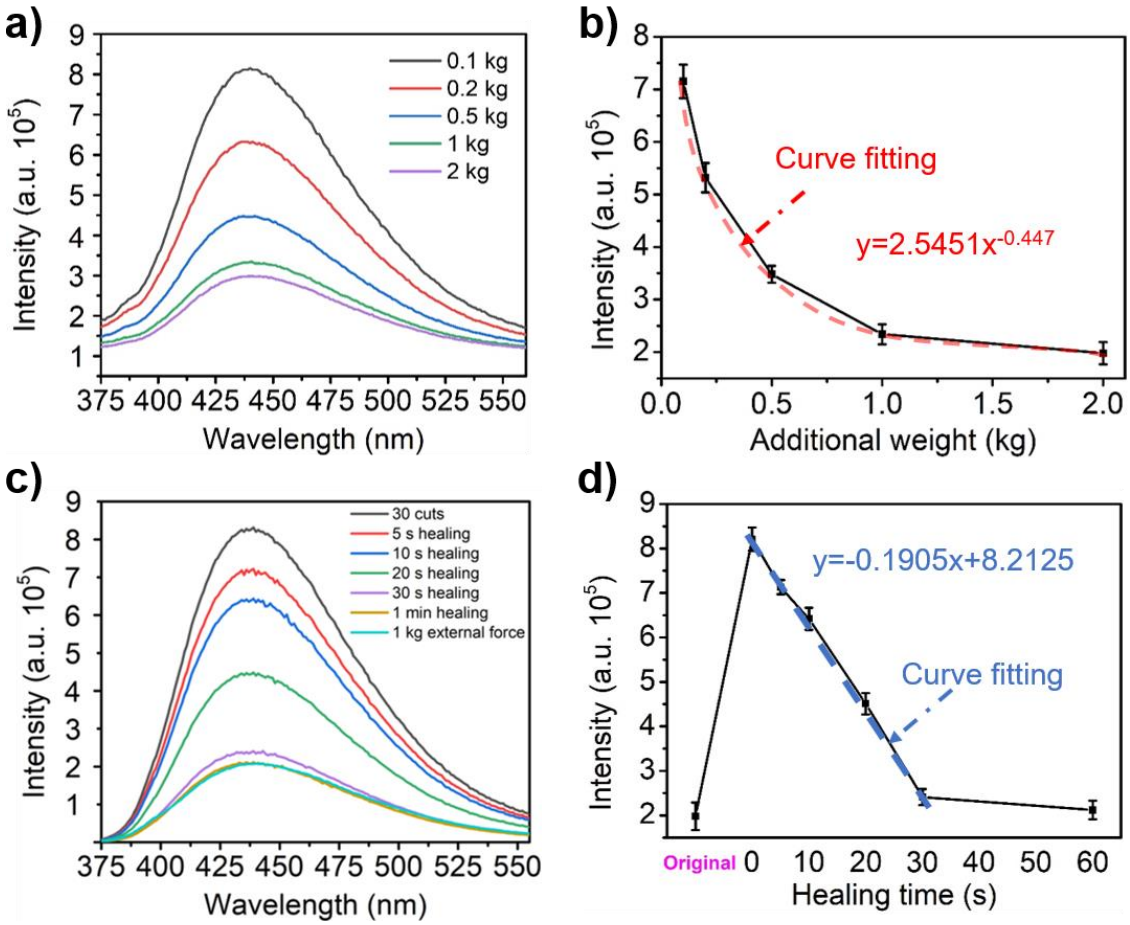

Figure S24. a) Relationship between the fluorescence intensity of hydrogel (doped with MXene quantum dots) and its state (original, cut, healed). b) A fitted curve between the fluorescence intensity of hydrogel (doped with MXene quantum dots) and its state (original, cut, healed). c) The relationship between the fluorescence intensity of hydrogel (doped with MXene quantum dots) and the external force to which hydrogel was subjected. d) A fitted curve between the fluorescence intensity of hydrogel (doped with MXene quantum dots) and the external force it was subjected to.

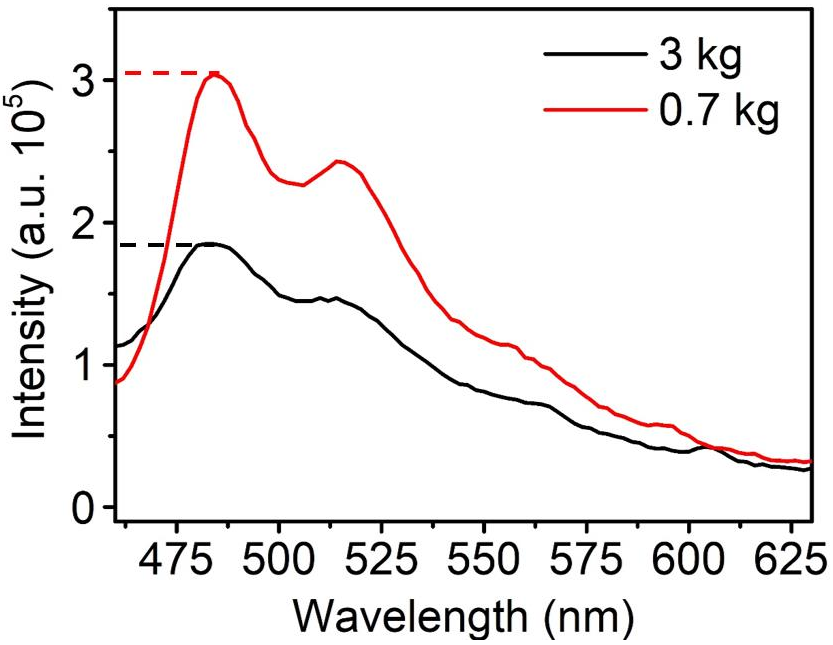

Figure S25. The relationship between the fluorescence intensity of the hydrogel (doped with carbon quantum dots) and the external force (3 kg; 0.7 kg) to which hydrogel was subjected.

Supplementary explanation

Figure S25 shows that the fluorescence excitation intensity of the hydrogel was approximately $3.1*10^5$ when the external force was 0.7 kg. The fluorescence excitation intensity of hydrogel was approximately $1.8*10^5$ when the external force was 3 kg. The corresponding fluorescence excitation intensity of hydrogel could be calculated using the external force by using the formula $y = 2.6234x^{-0.426}$, where y represents the fluorescence excitation intensity of hydrogel and x represents the external force that hydrogel received. According to formula $y = 2.6234x^{-0.426}$, when the external force is 0.7 kg/3 kg, the calculated fluorescence excitation intensity of hydrogel was $3.05*10^5/1.64*10^5$. These results were similar, so the formula is valid.

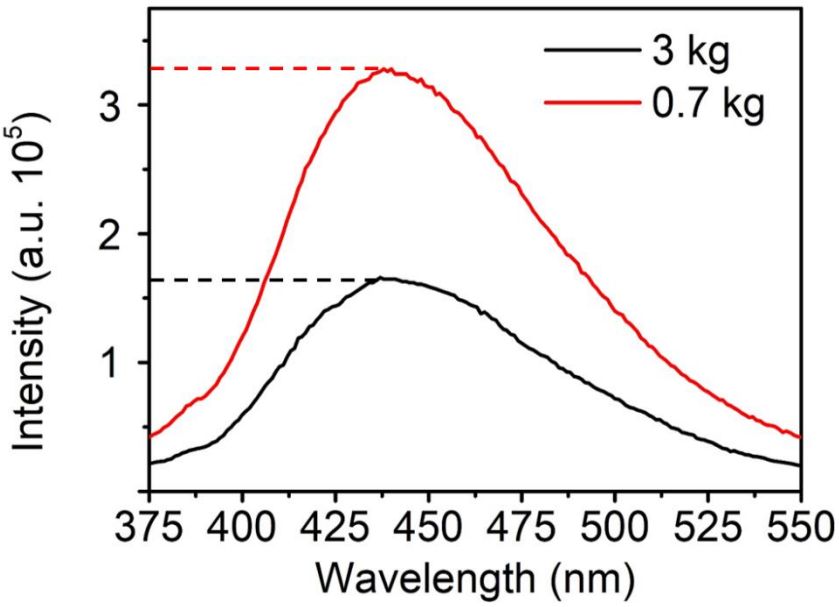

Figure S26. The relationship between the fluorescence intensity of hydrogel (doped with MXene quantum dots) and the external force (3 kg; 0.7 kg) to which hydrogel was subjected.

Supplementary explanation

Figure S26 shows that the fluorescence excitation intensity of hydrogel was approximately $3.15*10^5$ when the external force was 0.7 kg. The fluorescence excitation intensity of hydrogel was approximately $1.62*10^5$ when the external force was 3 kg. The corresponding fluorescence excitation intensity of the hydrogel was calculated using the external force with the formula $y = 2.5451x^{-0.447}$, where y represents the fluorescence excitation intensity of hydrogel and χ represents the external force that hydrogel received. According to formula $y = 2.5451x^{-0.447}$, when the external force was 0.7 kg/3 kg, the calculated fluorescence excitation intensity of the hydrogel was $2.985*10^5/1.558*10^5$. These results were similar, verifying the validity of the formula.

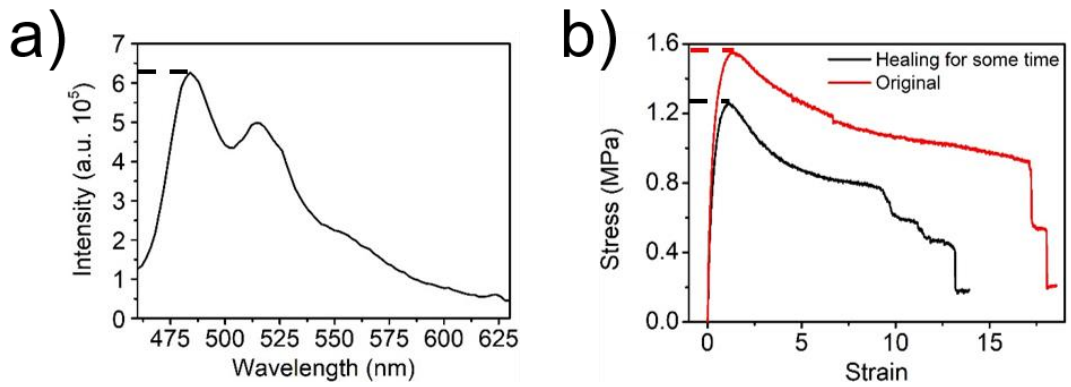

Figure S27. a) Fluorescence excitation intensity of hydrogel (doped with carbon quantum dots). b) Tensile stress-strain curves of the original hydrogel and the healed or self-repaired hydrogel (doped with carbon quantum dots).

Supplementary explanation

Figure S27a shows that the fluorescence excitation intensity of the hydrogel was approximately $6.25*10^5$. Figure 3e and Figure 2c show that the self-healing efficiency of the hydrogel was approximately 80%. The self-healing efficiency of the hydrogel from Figure S27b could be calculated using the following equation: $R=\delta_1/\delta_0*100\%=1.25/1.56*100\%=80.13\%$ R represents the self-healing efficiency of hydrogel, and δ_0 and δ_1 are the tensile stresses before and after the hydrogel underwent self-healing, respectively. These two different calculation methods had similar results, verifying the methodology using the fitted graph.

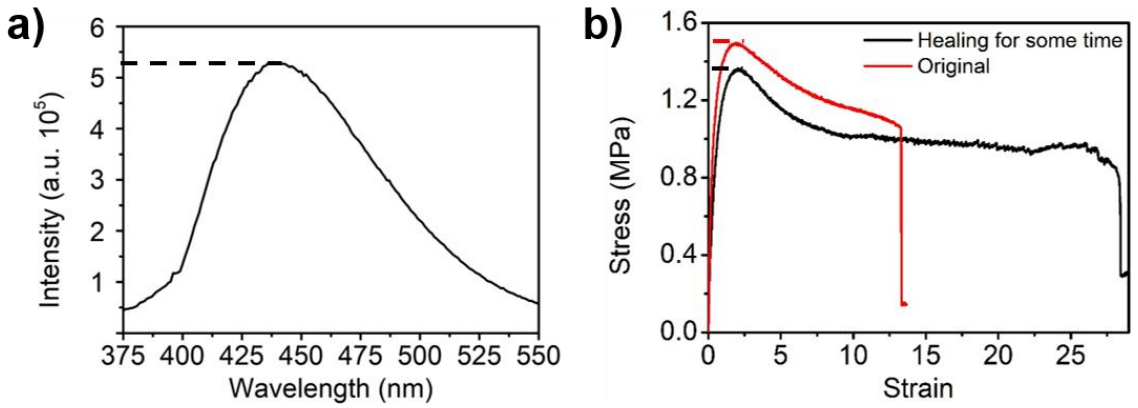

Figure S28. a) Fluorescence excitation intensity of hydrogel (doped with MXene quantum dots). b) Tensile stress-strain curves of original hydrogel and healing hydrogel (doped with MXene quantum dots).

Supplementary explanation

Figure S28a shows that the fluorescence excitation intensity of the hydrogel was approximately $5.15*10^5$. Figure S24d and Figure 2c showed that the self-healing efficiency of hydrogel was approximately 90%. The self-healing efficiency of the hydrogel from Figure S28b could be calculated using the following equation:. $R = \delta_1 / \delta_0 *100\%=1.37/1.51*100\%=90.73\%$, where R represents the self-healing efficiency of the hydrogel, and δ_0 and δ_1 are the tensile stresses before and after the hydrogel underwent self-healing, respectively. These two different calculation methods had similar results, verifying the methodology using the fitted graph.

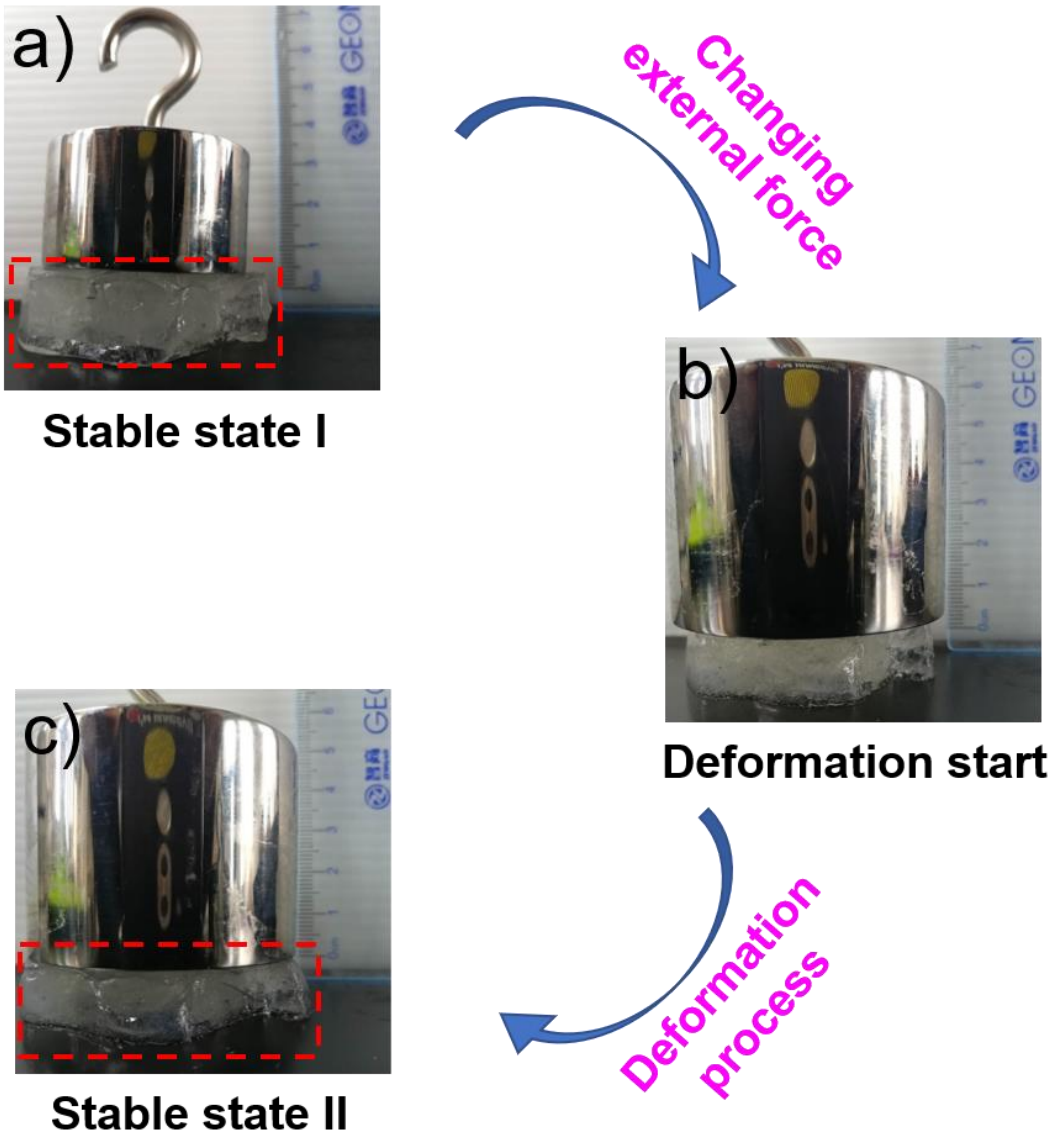

.

Figure S29. a) Stable status of hydrogel when the external force is 2kg. b) Replacing the 2 kg external force with 5 kg external force. c) Stable status of hydrogel when the external force is 5 kg.

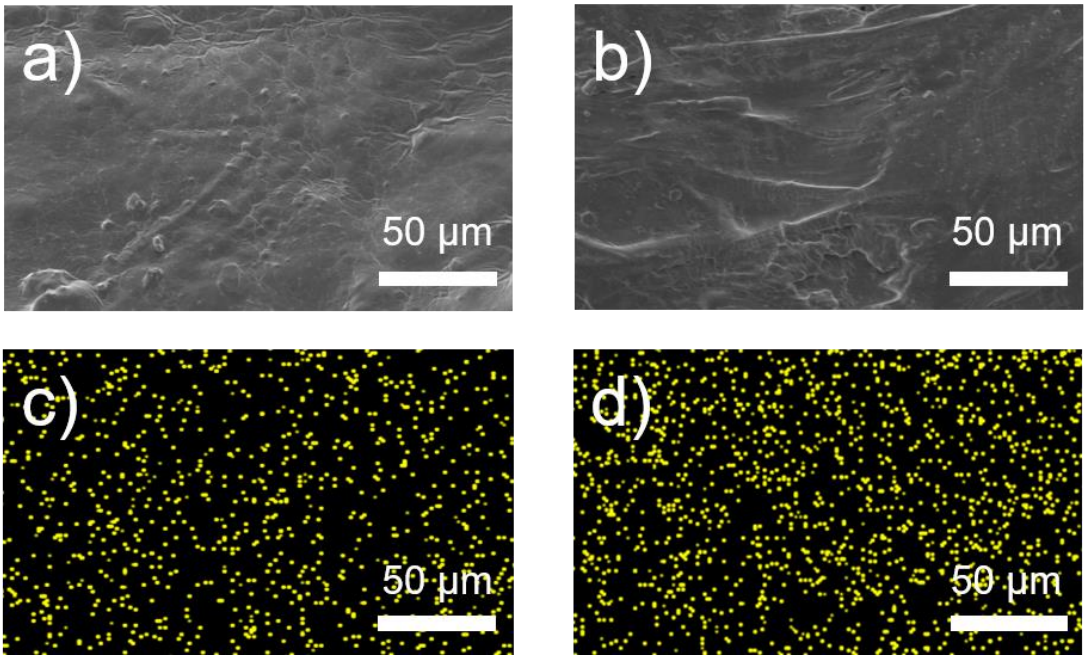

Figure S30. a) SEM image of hydrogel (2 kg external force). b) SEM image of hydrogel (5 kg external force). c) Distribution image of feature element Zn in hydrogel (image in Figure S30a). d) Distribution image of feature element Zn in hydrogel (image in Figure S30b).

Supplementary explanation

The raw materials (agarose, chitosan, PVA, glycerol, sodium tetraborate) used in the as-synthesized hydrogel only contained C, H, O, N, B and Na elements (Figure S3f). The Zn element is the feature element that we added to the blue quantum dots in order to determine the distribution of quantum dots in hydrogel. As can be seen from Figure S30c and S30d, the quantum dots density in the hydrogel are different. The greater the external force, the denser the distribution of quantum dots in the hydrogel.

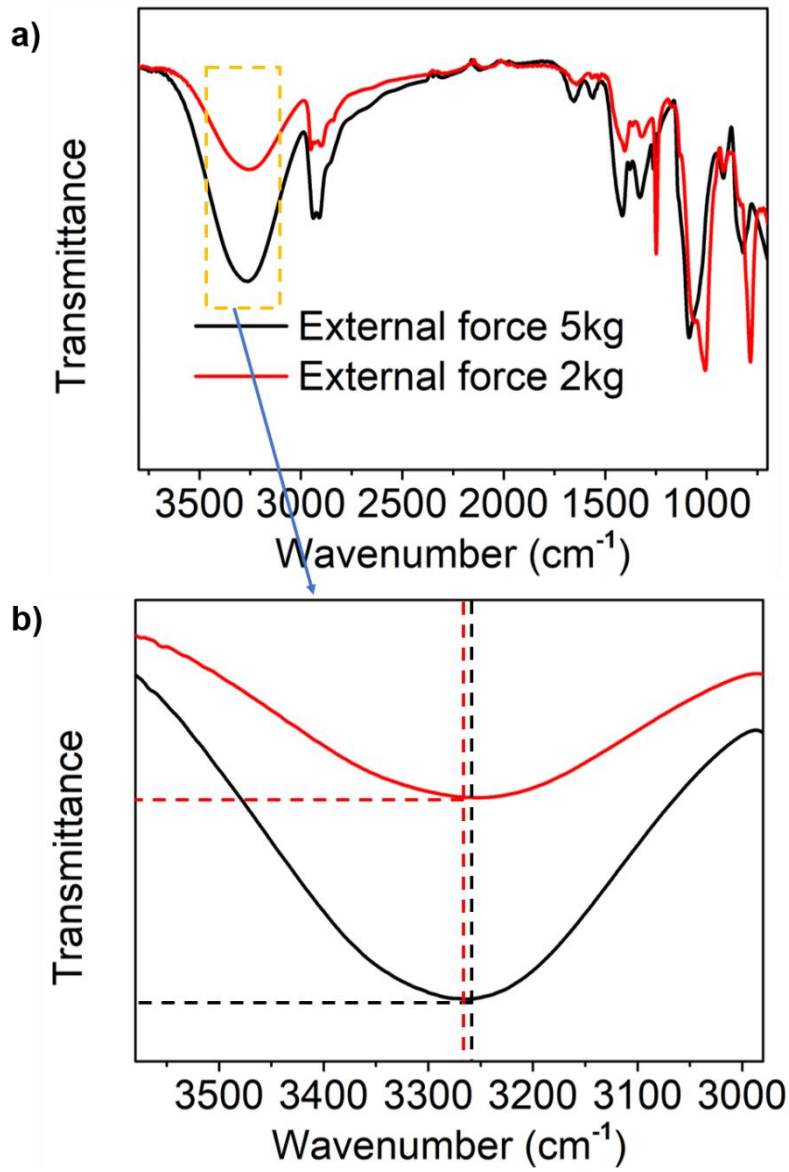

Figure S31. a) FTIR spectra of hydrogel with different external force. b) Partial enlargement of Figure S31a.

Supplementary explanation

Figure S31 shows the intensity (number) of hydrogen bond in hydrogel when it suffers from different external forces.

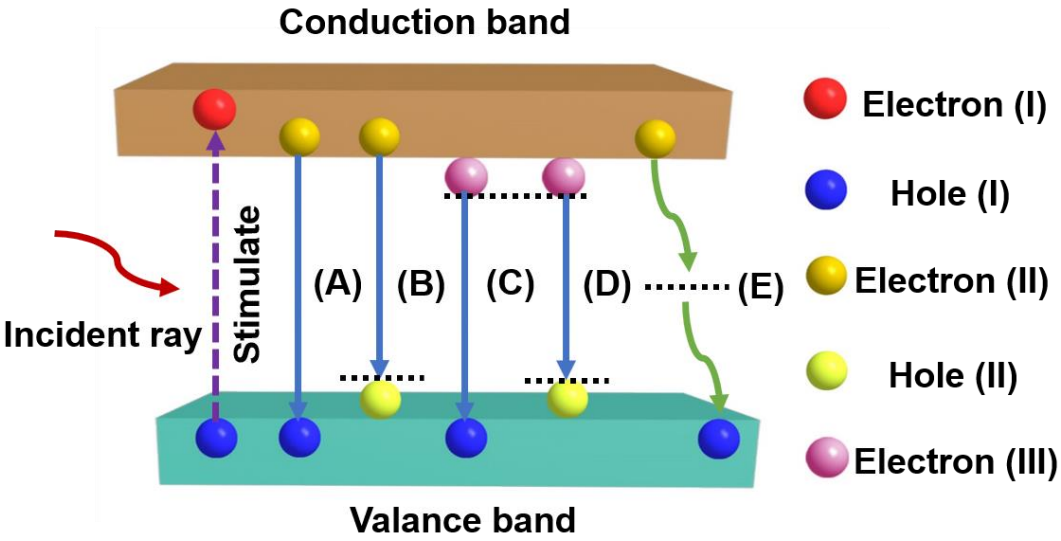

Figure S32. Fluorescence excitation diagram of quantum dots (carbon/MXene).

Supplementary explanation

Quantum dots move to an excited state after absorbing foreign photons, and the energy can be reverted back to the ground state in a variety of ways, through a process generally referred to as relaxation. In the majority of cases, when the atom returns to the ground state, the energy is lost to the surroundings as heat. However, in some other cases, the energy can be released in the form of photon emission. The fluorescence spectrum used in our tests involves the emission spectrum. The emission spectrum is the distribution of the fluorescence intensity at different wavelengths under the excitation light of a certain fixed wavelength. The position of the maximum fluorescence intensity in the emission spectrum is called λ_{max}, which is an important parameter of the fluorescence spectrum and is sensitive to the polarity of the environment and the movement of the fluorophore. Thus, this sensitivity to fluorophore motion allows us to use the fluorescence to detect the external forces and the self-healing efficiency of hydrogels.

References

1 W. P. Chen, D. Z. Hao, W. J. Hao, X. L. Guo, L. Jiang, *ACS Appl. Mater. Interfaces*, 2017, **10**, 1258-1265.

2 G. Weng, S. Thanneeru, J. He, *Adv. Mater.*, 2018, **30**, 1706526.

3 Y. J. Liu, W. T. Cao, M. G. Ma, P. Wan, *ACS Appl. Mater. Interfaces*, 2017, **9**, 25559-25570.

4 Z. Wei, J. H. Yang, Z. Q. Liu, F. Xu, J. X. Zhou, M. Zrínyi, Y. Osada, Y. M. Chen, *Adv. Funct. Mater.*, 2015, **25**, 1352-1359.

5 T. L. Sun, T. Kurokawa, S. Kuroda, A. B. Ihsan, T. Akasaki, K. Sato, M. A. Haque, T. Nakajima, J. P. Gong, *Nat. Mater.*, 2013, **12**, 932.

6 B. C. Tee, C. Wang, R. Allen, Z. Bao, *Nat. Nanotechnol.*, 2012, **7**, 825.

7 L. Li, B. Yan, J. Yang, L. Chen, H. Zeng, *Adv. Mater.*, 2015, **27**, 1294-1299.

8 I. Jeon, J. Cui, W. R. Illeperuma, J. Aizenberg, J. J. Vlassak, *Adv. Mater.*, 2016, **28**, 4678-4683.

9 F. Chen, Q. Chen, L. Zhu, Z. Q. Tang, Q. F. Li, G. Qin, J. Yang, Y. X. Zhang, B. P. Ren, J. Zheng, *Chem. Mater.*, 2018, **30**, 1743-1754.

10 W. Sun, B. Xue, Y. Li, M. Qin, J. Wu, K. Lu, J. Wu, Y. Cao, Q. Jiang, W. Wang, *Adv. Funct. Mater.*, 2016, **26**, 9044-9052.

11 Y. Ohsedo, M. Taniguchi, K. Saruhashi, H. Watanabe, *RSC Adv.*, 2015, **5**, 90010-90013.

12 Y. Mao, T. Su, Q. Wu, C. Liao, Q. Wang, *Chem. Commun.*, 2014, **50**, 14429-14432.

13 T. Kataoka, Y. Ishioka, M. Mizuhata, H. Minami, T. Maruyama, *ACS Appl. Mater. Interfaces*, 2015, **7**, 23346-23352.

14 Q. Wei, M. Xu, C. Liao, Q. Wu, M. Liu, Y. Zhang, C. Wu, L. Cheng, Q. Wang, *Chem. Sci.*, 2016, **7**, 2748-2752.

15 M. A. Haque, T. Kurokawa, G. Kamita, J. P. Gong, *Macromolecules*, 2011, **44**, 8916-8924.

16 S. E. Bakarich, G. C. Pidcock, P. Balding, L. Stevens, P. Calvert, M. Panhuis, *Soft Matter*, 2012, **8**, 9985-9988.

17 J.-Y. Sun, X. Zhao, W. R. Illeperuma, O. Chaudhuri, K. H. Oh, D. J. Mooney, J. J. Vlassak, Z. Suo, *Nature*, 2012, **489**, 133.

18 Q. Chen, L. Zhu, C. Zhao, Q. Wang, J. Zheng, *Adv. Mater.*, 2013, **25**, 4171-4176.